Correlations in the thermal fluctuations of free-standing smectic-*A* films as measured by x-ray scattering

E. A. L. Mol, J. D. Shindler, A. N. Shalaginov,* and W. H. de Jeu
FOM Institute for Atomic and Molecular Physics, Kruislaan 407, 1098 SJ Amsterdam, The Netherlands
(Received 8 November 1995)

The displacement-displacement correlations in the thermal fluctuations of freely suspended smectic-*A* films of 3 to 34 layers have been determined using small angle specular and diffuse x-ray scattering. By choosing a symmetric resolution a simple separation of the resolution function into contributions parallel and perpendicular to the wave vector transfer is possible. This enables modeling of the scattered intensity without introducing an artificial separation of the specular and diffuse contribution. The data are interpreted using a continuous model to describe the displacement-displacement correlations, which is shown to be equivalent to the original discrete model of Holyst [Phys. Rev. A **44**, 3692 (1991)], but computationally more efficient. Two characteristic in-plane lengths are introduced: R_l, above which the distance dependence of the correlation function follows a logarithmic law, and R_c, above which the layers throughout the film fluctuate in unison, i.e., conformally. Values for the smectic bend and compression elastic constants as well as the surface tension are obtained from the wavelength dependence of the correlations. The fluctuation profile depends only slightly on the film thickness and is nearly flat for the fluorinated compound investigated. All films investigated are conformal down to the smallest in-plane length scales measured. Furthermore, the collective long wavelength thermal fluctuations, which only depend on the diffuse scattering, can be separated from the local smectic disorder. The local contribution to the total fluctuation profile is found to be considerable. [S1063-651X(96)02206-4]

PACS number(s): 61.30.Cz, 68.15.+e, 61.10.−i, 05.40.+j

I. INTRODUCTION

Smectic liquid crystals are characterized by long-range orientational order of the elongated molecules and reduced positional order. The translational order is lost in the two directions perpendicular to **n**, the axis of preferred orientation. However, parallel to **n** the molecular centers are on average arranged in equidistant layers, thus forming a one-dimensional crystal. Since such a system is at its lower marginal dimensionality, the translational order is not truly long range but decays algebraically with position as $\mathbf{r}^{-\eta}$. In the case of true long-range order the positional correlation between two layers would approach a constant if the layers are infinitely far apart. The fluctuations of the smectic layers are responsible for the absence of true long-range order. If $u(\mathbf{r})$ is the layer displacement from its equilibrium position, $\langle u^2(\mathbf{r})\rangle$ is found to diverge logarithmically with the sample size (Landau-Peierls instability) [1]. In practice it is difficult to observe the loss of long-range order because of the slow logarithmic growth of the fluctuations with the size of the sample [2].

Due to their layered structure smectic liquid crystals can form films that are freely suspended over an aperture in a frame. This property of smectics has been known since the beginning of this century [3], but the interest in freely suspended smectic films was renewed in the seventies by the optical experiments of Young *et al.* [4] and Rosenblatt *et al.* [5] These experiments were followed by numerous calorimetric, mechanical, hydrodynamical, and x-ray studies, a number of which are collected in Ref. [6]. Freely suspended films have a controlled size and high degree of uniformity. The thickness can vary from 2 to over 200 layers, thus allowing us to investigate the crossover from three-dimensional to two-dimensional behavior, as well as the influence of the surfaces on the physical properties.

Recently theoretical models of free-standing smectic films have been developed [7–11], that extend the smectic bulk free energy, which depends on the elastic constants for compression B and bending K of the smectic layers, to include the effect of surface tension γ at the interfaces. Central to the theory is the calculation of the layer displacement function $\sigma^2(0,z)=\langle u^2(0,z)\rangle$ and of the displacement-displacement correlation function $C(R,z,z')=\langle u(\mathbf{R},z)u(0,z')\rangle$, where $\mathbf{r}=(\mathbf{R},z)$ with $\mathbf{R}$ in the plane of the film and z along the film normal. The original formulation by Holyst [8] uses discretized fluctuations as a function of z. A later continuous version [9] has been shown to be equivalent. In this article we elaborate on a different continuous version of the theory developed in [10], which is computationally most efficient. The equivalence of these various models is shown explicitly in the Appendix.

Free-standing smectic films can be made large and flat enough for measurements of the x-ray reflectivity [12–14], which probes the laterally averaged density profile through the film. Recently, we extended this type of measurement to include the nonspecular diffuse scattering [15], which allows a direct determination of the displacement-displacement correlation function. Measurements of the diffuse scattering have been used to gain insight into the lateral distribution of surface undulations of liquid [16,17] and solid [18–22] surfaces, black soap films [23], and smectic liquid crystal poly-

*Present address: Faculty of Mathematical Studies, University of Southampton, Southampton SO17 1BJ, United Kingdom.

mer films on a substrate [24,25]. In the last case the layer fluctuations were dominated by the static undulations of the underlying substrate.

In the case of freely suspended smectic films the diffuse scattering probes the in-plane wave vector dependence of the long-wavelength thermal fluctuations. This enables the determination of the interlayer displacement-displacement correlation function, without assumptions about the local layer structure. From $C(R,z,z')$ values for the surface tension and the elastic constants of the smectic layers can be derived. Once this is known, we obtain from the specular x-ray reflectivity the local (uncorrelated) contribution of the smectic disorder to the total fluctuation profile. Thus the extent of local smectic disorder and the magnitude of the long length scale thermal fluctuations can be separated by the combination of specular *and* diffuse x-ray reflectivity measurements. We find the local contribution to be non-negligible for the fluorinated compound investigated, contrary to the usual assumption.

At long in-plane length scales the thermal fluctuations are highly correlated as a result of the slow algebraic decay of the interlayer density-density correlation function. The layers fluctuate conformally, i.e., they undulate in unison. In this case the diffuse scattering is the coherent superposition of scattering from each layer and will show maxima and minima at the same positions as the specular reflectivity. The shorter the in-plane length scale and the thicker the film, the more likely it is to lose this conformality. All investigated films (up to 34 layers) of the fluorinated compound used are conformal at the in-plane length scales measured.

Following the preliminary results given in Ref. [15] we start in the next section with a full account of the theory. In Sec. III the experimental details are given, which includes a discussion of the specific choices for the resolution that are required to analyze the data quantitatively. Section IV presents the experimental results and fitting parameters, followed by a discussion in Sec. V.

II. THEORY

The free energy for a free-standing smectic film can be written as the sum of a bulk contribution [26].

$$F_B=\frac{1}{2}\int d^3r\left[B\left[\frac{\partial u(\mathbf{r})}{\partial z}\right]^2+K[\Delta_\perp u(\mathbf{r})]^2\right] \tag{1}$$

and a surface contribution [8],

$$F_S=\frac{1}{2}\gamma\int d^2r[[\nabla_\perp u(\mathbf{R},z=L/2)]^2 + [\nabla_\perp u(\mathbf{R},z=-L/2)]^2]. \tag{2}$$

The surface terms describes the energy cost associated with increasing the surface area of the two free surfaces located at $z=L/2$ and $z=-L/2$, where $L=Nd$ is the thickness of a film of N layers with layer spacing d. Within the framework of the theory, bulk elastic constants are used; therefore the values of B and K should be independent of the layer number and the film thickness.

The calculation of $\langle u^2(0,z)\rangle$ and of $C(R,z,z')=\langle u(\mathbf{R},z)u(0,z')\rangle$ is central to the theoretical formalism. The case $\mathbf{R}=\mathbf{0}$ reveals information about the compressional modes, that depend on B. By studying $C(R,z=z')$ information about undulations (and thus K) can be obtained. The fluctuation profile depends upon the ratio $\nu=\gamma/\sqrt{KB}$; for $\nu>1$ surface damping of the fluctuations is expected, while for $\nu<1$ the fluctuations amplitudes will be enhanced at the surfaces. In this section we present an extension of the theory developed in Ref. [10].

In the original analysis by Holyst [8] two regimes are obtained for the R dependence of $C(R,z,z')$. At short distances R a strong dependence of $C(R,z,z')$ on the layer position is found. At large separation all the layers fluctuate in unison, i.e., conformally, and $C(R,z,z')$ decays logarithmically with increasing R. Qualitatively the two regimes can be understood as follows. In a bulk smectic liquid crystal a distortion with an in-plane wave number $Q=2\pi/R$ decays slowly from one layer to the other, due to the small compressibility of the system in the z direction. The characteristic decay length of the distortion is given by $l(Q)=1/(\lambda Q^2)$, where $\lambda=\sqrt{K/B}$ [26]. Therefore within this approximation a film is expected to fluctuate conformally for $R>R_c=2\pi\sqrt{L\lambda}$ as determined by $l(Q)=L$. Although this argument explains, in principle, the two regimes and gives R_c for a thick film, it does not provide the proper value of R_c in a thin film, in which case the surface tension must be taken into account.

To find out how the surface tension affects R_c in a free-standing film we consider the first principal mode of the fluctuations, which gives the main contribution to the correlation function (see the Appendix). It corresponds to the smallest eigenvalue of the operator defined by Eq. (A8) in the Appendix. Higher modes can be disregarded when the difference between the second and the first eigenvalue is larger than the first eigenvalue. As this difference is proportional to L^{-2} [10], the following consideration is valid only for thin films. The mode with the lowest eigenvalue can be written as $\cos(\kappa z)$. The layers can be expected to fluctuate conformally if $\cos(\kappa z)$ does not change considerably across the film, i.e., if $\kappa L\ll 2\pi$. From Eq. (A9) κ is given by the minimal positive root of

$$\frac{\gamma Q^2}{B\kappa}=\tan(\kappa L/2). \tag{3}$$

To locate the boundary of the real-space range of conformality we use $\tan(\kappa L/2)\approx\kappa L/2$ and $Q\approx 2\pi/R$. This yields

$$R\gg R_c\approx\sqrt{2\gamma L/B}. \tag{4}$$

If we take $L=1830$ Å, $K=10^{-11}$ N, $B=2.5\times10^6$ N/m^2 and $\gamma=30\times10^{-3}$ N/m, Eq. (4) gives $R_c=660$ Å which is consistent with the numerical result for the same parameters shown in Fig. 1 of Ref. [8]. In the limiting cases of infinite B (a fully incompressible film) and zero B, R_c is equal to zero and infinity, respectively, as to be expected. The ratio $\varrho_c=R_c/\sqrt{L\lambda}$ is a function of ν and equals $\sqrt{2\nu}$ according to Eq. (4).

To calculate the displacement-displacement correlation function we follow Ref. [10]. Instead of $C(R,z,z')$ we will use the full correlation function

$$g(R,z,z') = \langle [u(\mathbf{R},z) - u(0,z')]^2 \rangle = \sigma^2(\mathbf{R},z) + \sigma^2(0,z') - 2C(R,z,z'). \quad (5)$$

While each of the right-hand terms diverges with increasing film size and, thus, requires an additional cutoff, this is not the case for $g(R,z,z')$. It can be written in the following form (see the Appendix):

$$g(R,z,z') = \frac{k_B T}{8\pi\sqrt{KB}} \int_0^{\xi_0} d\xi \times \frac{1}{\xi[(1+\nu)^2 - (1-\nu)^2 \exp(-2\xi)]} \times [f(\xi,2z,z_0) + f(\xi,2z',z_0) - 2J_0(\varrho\sqrt{\xi}) f(\xi,z_+,z_-)], \quad (6)$$

where $\xi = L\lambda Q^2$, $\xi_0 = L\lambda(2\pi/a_0)^2$, a_0 is a lateral intermolecular distance, $z_+ = z + z'$, and $z_- = |z - z'|$ (with minimal value z_0) and $\varrho = R/\sqrt{\lambda L}$. J_0 is the Bessel function of order zero, while the function f is given by

$$f(\xi,z_+,z_-) = 2(1-\nu^2)\exp(-\xi)\cosh(\xi z_+/L) + (1+\nu)^2 \times \exp(-\xi z_-/L) + (1-\nu)^2 \times \exp[-\xi(2 - z_-/L)]. \quad (7)$$

A cutoff chosen as $z_0 \simeq d/4$ reproduces essentially the results from the discrete model of Holyst [8]. Also, for the choice of $z_0 > a_0$, the correlation function is not sensitive to the value of a_0, because the integrand decays exponentially. This allows us to expand the integration to infinity and, as a consequence, eliminates the second cutoff ξ_0. Now the integration in Eq. (6) can be carried out analytically, using the following identities

$$\frac{1}{(1+\nu)^2 - (1-\nu)^2 \exp(-2\xi)} = \frac{1}{(1+\nu)^2} \sum_{n=0}^{\infty} \left(\frac{1-\nu}{1+\nu}\right)^{2n} e^{-2n\xi}$$

and

$$\int_0^{\infty} dv\, \frac{1}{v} [e^{-\alpha v} - e^{-\beta v} J_0(\varrho\sqrt{v})] = A\left(\frac{\varrho^2}{4\beta}\right) + \ln\left(\frac{\beta}{\alpha}\right), \quad (8)$$

where

$$A(w) = \ln(w) + E_1(w) + c$$

and E_1 is the exponential integral function and c Euler's constant ($c = 0.5772\ldots$). This leads to the following expression for the correlation function:

$$g(R,z,z') = \frac{k_B T}{8\pi\sqrt{KB}(1+\nu)^2} \sum_{n=0}^{\infty} \left(\frac{1-\nu}{1+\nu}\right)^{2n} \Bigg\{ (1-\nu^2) \times \Bigg[\ln\left(\frac{1+z_+/L+2n}{1+2z/L+2n}\right) + \ln\left(\frac{1+z_+/L+2n}{1+2z'/L+2n}\right) + \ln\left(\frac{1-z_+/L+2n}{1-2z/L+2n}\right) + \ln\left(\frac{1-z_+/L+2n}{1-2z'/L+2n}\right) + 2A\left(\frac{\varrho^2}{8n+4+4z_+/L}\right) + 2A\left(\frac{\varrho^2}{8n+4-4z_+/L}\right) \Bigg] + 2(1+\nu)^2 \times \left[\ln\left(\frac{z_-/L+2n}{z_0/L+2n}\right) + A\left(\frac{\varrho^2}{4z_-/L+8n}\right) \right] + 2(1-\nu)^2 \Bigg[\ln\left(\frac{2-z_-/L+2n}{2-z_0/L+2n}\right) + A\left(\frac{\varrho^2}{8+8n-4z_-/L}\right) \Bigg] \Bigg\}. \quad (9)$$

Equation (9) is the expression for the correlation function used in the analysis of the experimental results.

In the particular case of $\gamma = \sqrt{KB}$ Eq. (9) yields

$$g(R,z,z') = \frac{k_B T}{4\pi\gamma} \left[\ln\left(\frac{R^2}{4\lambda z_0}\right) + E_1\left(\frac{R^2}{4\lambda z_-}\right) + c \right]. \quad (10)$$

The right-hand side of Eq. (10) does not depend on $z + z'$ and therefore the profile is completely flat (see also Ref. [10]). As a consequence information about the film thickness is lost; Eq. (10) does not contain L. It means that the smectic film can be described as if it were cut from a bulk smectic liquid crystal with a surface tension equal to $\sqrt{KB}$. The corresponding expression for a bulk smectic-A sample was derived for the first time by Caillé [27]. The two expressions coincide for $z_0 = d^2 e^{-c}/\lambda$. Equation (10) is also similar to an equation derived in Ref. [28] for an infinite sample with the assumption $z_- \gg d$. A proper choice of z_0 makes them identical. While in Eq. (10) the cutoff is constant, the corresponding implicit z_0 in Ref. [28] depends on all the other parameters. For $d = 30$ Å, $K = 10^{-11}$ N, and $a_0 = 4$ Å the ratio d/z_0 is found to vary from 5.0 to 2.3 when B changes from 10^7 to 10^9 N/m^2. Thus this dependence does not result in a large variation. Our choice of z_0, as a cutoff parameter analogous to a_0, is explained in the Appendix. The exponential decay of E_1 makes the second term in Eq. (10) negligible if the argument is larger than 1. For this range of R we find that $g(R,z,z')$ depends neither on z nor z', but varies logarithmically with R. Since $z_- < L$, this range can be estimated as $R \ll R_l = 2\sqrt{L\lambda}$, still for $\nu = 1$.

In order to determine the range of R where $g(R,z,z')$ increases as $\ln(R)$ we return to Eq. (9), the full expression for the correlation function, for arbitrary values of ν. The logarithmic dependence can be written as $\partial_R g(R,z,z') \sim R^{-1}$. Differentiating Eq. (9) and using

$$\frac{\partial A(c\varrho^2)}{\partial \varrho}=\frac{2}{\varrho}\,(1-\exp(-c\varrho^2))$$

we obtain

$$\begin{aligned}\frac{\partial g(R,z,z')}{\partial R}=&\frac{k_BT}{2\pi\sqrt{KB}(1+\nu)^2}\,\frac{1}{R}\\&\times\left\{\frac{(1+\nu)^2}{\nu}-\sum_{n=0}^{\infty}\left(\frac{1-\nu}{1+\nu}\right)^{2n}\right.\\&\times\left[(1-\nu^2)\exp\left(-\frac{\varrho^2}{8n+4+4z_+/L}\right)\right.\\&+(1-\nu^2)\exp\left(-\frac{\varrho^2}{8n+4-4z_+/L}\right)\\&+(1+\nu)^2\exp\left(-\frac{\varrho^2}{8n+4z_-/L}\right)\\&\left.\left.+(1-\nu)^2\exp\left(-\frac{\varrho^2}{8n+8-4z_-/L}\right)\right]\right\}.\end{aligned}\tag{11}$$

The derivative $\partial_R g(R,z,z')$ is proportional to R^{-1} and at the same time independent of z and z' if the result of the summation within the braces is much smaller than the preceding term. In that case Eq. (11) simplifies to

$$\frac{\partial g}{\partial R}=\frac{k_BT}{2\pi\gamma R}.\tag{12}$$

Integration leads to

$$g(R,z,z')=\frac{k_BT}{2\pi\gamma}\ln(R/\sqrt{L\lambda})+D(z,z')\tag{13}$$

where $D(z,z')$ is independent of R. As we shall see in the analysis of the experiments, the prefactor defines the slope of a transverse diffuse scan in the appropriate region of R.

To determine the range of R where Eq. (13) applies the summation in Eq. (11) must be carried out. Analytically this is hardly possible, but some analysis can be done. In a narrow region around $\nu\approx 1$ the term with $n=0$ gives the main contribution to the infinite sum. Taking only this term into account we arrive at the condition $\exp(-\varrho^2/4)\ll 1$ for the required range. It provides the same R_l as calculated from Eq. (10). If ν differs considerably from 1, the sum converges slowly and the main contribution comes from the tail of the sum. In this case terms in the denominators, that are small compared to $8n$, can be neglected. Using in addition

$$\begin{aligned}\sum_{n=0}^{\infty}\exp(-an-b/n)&\approx\int_0^{\infty}dx\,\exp(-ax-b/x)\\&=2\sqrt{(b/a)}K_1(2\sqrt{ab}),\end{aligned}$$

where

$$a=2\ln\left|\frac{1+\nu}{1-\nu}\right|,\quad b=\frac{\varrho^2}{8},$$

the required condition for the logarithmic behavior of $g(R,z,z')$ can be written as

$$\frac{2\varrho\nu}{(1+\nu)^2\sqrt{\ln|(1+\nu)/(1-\nu)|}}\,K_1\left(\varrho\left[\ln\left|\frac{1+\nu}{1-\nu}\right|\right]^{1/2}\right)\ll 1.\tag{14}$$

Since the modified Bessel function in Eq. (14) contains an exponential decay as its argument gets larger, we arrive at

$$R_l\approx\left(\frac{L\lambda}{\ln|(1+\nu)/(1-\nu)|}\right)^{1/2}.\tag{15}$$

In the limiting case of $B\to\infty$ Eq. (15) evolves into

$$R_l\approx\left(\frac{LK}{2\gamma}\right)^{1/2},\tag{16}$$

and when $B\to 0$ we find

$$R_l\to\left(\frac{L\gamma}{2B}\right)^{1/2}.\tag{17}$$

An expression much simpler than Eq. (9) can be derived for incompressible free-standing smectic films. Taking in Eq. (6) the limit $B\to\infty$ one gets

$$g(R,z,z')=g(R)=\frac{k_BT}{2\pi\gamma}\int_0^{R_0q_m}dv\;\frac{1-J_0(Rv/R_0)}{v(1+v^2)},\tag{18}$$

where $q_m=2\pi/a_0$, $R_0=\sqrt{LK/(2\gamma)}$, and $v=R_0Q$. For a thin film of four layers with $d=30$ Å, $K=10^{-11}$ N, $\gamma=30\times10^{-3}$ N/m, and $a_0=4$ Å we find $R_0q_m\approx 10$. Thus, keeping in mind that the integrand decays as v^{-3}, we can replace the upper limit by infinity, except for the case of very thin films. With the expansion

$$\begin{aligned}\int_0^{\infty}dv\;\frac{1-J_0(\varrho v)}{v(1+v^2)}=\int_0^{\infty}dv\left\{\frac{vJ_0(\varrho v)}{1+v^2}+\frac{\cos(\varrho v)-J_0(\varrho v)}{v}\right.\\-\frac{1}{v}\left[\cos(\varrho v)-\frac{1}{1+\varrho^2v^2}\right]\\\left.+\frac{1}{v}\left[\frac{1}{1+v^2}-\frac{1}{1+\varrho^2v^2}\right]\right\},\end{aligned}$$

the integration can be carried out analytically. Using Ref. [29] to evaluate the first three terms we finally arrive at

$$g(\mathbf{R})=\frac{k_BT}{2\pi\gamma}\left[\ln(R/R_0)+K_0(R/R_0)+c-\ln(2)\right],\tag{19}$$

where K_n is the modified Bessel function of order n. It is easy to see that due to a fast decay of K_0 in this situation $R_c=0$ and R_l coincides with R_0. This is in agreement with Eq. (16) given above. Note that the prefactor is the same as in Eq. (13).

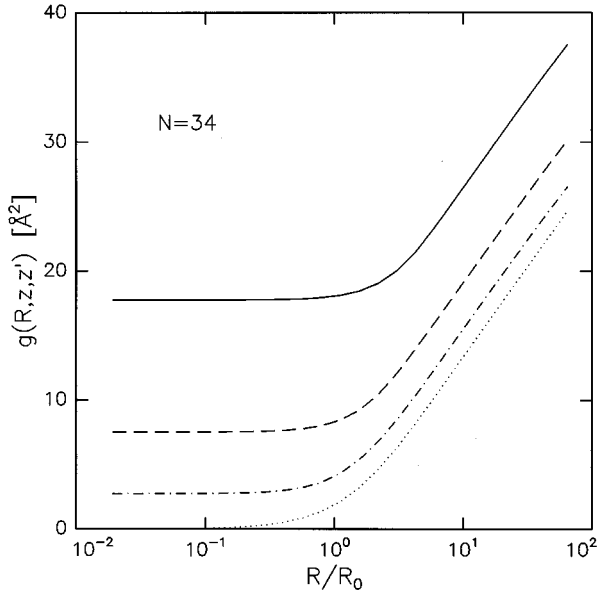

FIG. 1. The full correlation function versus R/R_0. R_0 is defined below Eq. (18); z and z' correspond to the top and bottom layers, respectively. The calculation is for a 34-layer film with $\gamma=13.0\times10^{-3}$ N/m, $K=10^{-11}$ N and $d=29.4$ Å. The four curves, from top to bottom, correspond to B is 10^7 N/m^2, 10^8 N/m^2, 10^9 N/m^2 and ∞, respectively.

Figure 1 shows the dependence of $g(R,z,z')$ on R calculated numerically on the basis of Eq. (6) and Eq. (19) for various values of B. The straight lines correspond to the logarithmic law for the correlation function. The characteristic length R_l that limits this region starts at $R_l=R_0$ for infinite B and increases with decreasing values of B.

In summary we find that in general two characteristic in-plane lengths are needed to describe the fluctuations: R_l and R_c. For $R>R_l$ the correlation function has a logarithmic dependence on R and for $R>R_c$ the layers undulate conformally. In the case of a thin film the surface tension strongly affects the fluctuations and $R_c=\sqrt{2\gamma L/B}$ (Eq. 4). If $\gamma \approx \sqrt{KB}$ we find $R_l \approx R_c \approx 2\sqrt{L\lambda}$. Equations (16) and (17) show how R_l depends on the physical parameters when the surface tension is much smaller and much larger than $\sqrt{KB}$, respectively. If B tends to infinity, R_c tends to zero, but R_l is finite. In the opposite range of B where $\nu \geqslant 1$, R_c and R_l are approximately equal. The prefactor $k_BT/2\pi\gamma$ in the logarithmic region of the correlation function does not depend on the elastic parameters K and B, but is only affected by the surface tension.

III. EXPERIMENT

A. Sample preparation

The compound investigated, 4-heptyl-2-[4-(2-perfluorhexylethyl)phenyl]-pyrimidin (FPP), is pictured in Fig. 2(a) where the phase sequence is also given. FPP was obtained from Merck (Darmstadt, Germany), and was used without further purification. FPP was chosen because the fluorinated tail causes the density variations along the molecule to be large and asymmetric, producing strong Bragg peak scattering and, in particular, a strong second order peak.

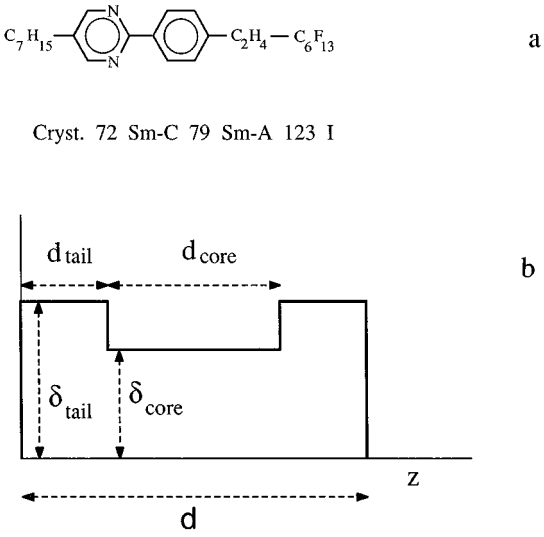

FIG. 2. (a) The chemical structure of FPP; (b) The model for a single smectic layer.

The films covered an area of 28×10 mm^2 determined by four razor blades spotwelded on the edges of a rectangular hole in a polished stainless steel plate. They were drawn manually at 120–123 °C by moving a wiper with a narrow slit, which was filled with liquid crystal, over the hole. The sample holder was mounted in a rectangular, copper sample cell with inner dimensions of $40\times24\times10$ mm^3. The cell has kapton windows allowing the incident and the reflected x-ray beam to pass at angles between 0 and 12°. The film holder was centered at the middle of the cell by pressing the backplate below the holder against the cover of the cell with a screw. The sample cell was contained in a vacuum tight aluminum outer oven with Mylar windows. The temperature of both cell and oven was measured with platinum resistors and controlled independently by heating resistors attached to the respective outer walls. Temperatures were regulated using Eurotherm PID controllers to within 0.1°. Measurements were performed at 88 °C, well in the smectic-*A* phase. Directly after creation the film generally consisted of regions of different thicknesses. After several hours of equilibration the final film thickness was achieved. The thickness was constant during the experiment, as checked by scanning part of the specular reflectivity every day. All but the thinnest film were stable for more than a week.

B. Scattering configuration

Cu-K_α x-rays were obtained from a Rigaku RU-300H generator operated at 18 kW maximum power. The wave vector is given by $\mathbf{k}$, with $|\mathbf{k}|=4.075$ Å^{-1}. Measurements were made using the geometry shown in Fig. 3(a). It employs a bent pyrolytic graphite (002) monochromator (20×20 mm^2, 115 mm radius), which focuses the beam in the out-of-plane direction onto the sample. Both Cu-$K_{\alpha1}$ and Cu-$K_{\alpha2}$ lines are selected in this moderate resolution setup [30]. A schematic of the scattering geometry is depicted in Fig. 3(b), where α and β are the angles of the incoming and outgoing wave vectors with respect to the surface.

The incident in-plane divergence $\Delta\alpha$ is defined by slits $S1$ and $S2$, set at 0.3 mm and 0.05 mm, respectively, and sepa-

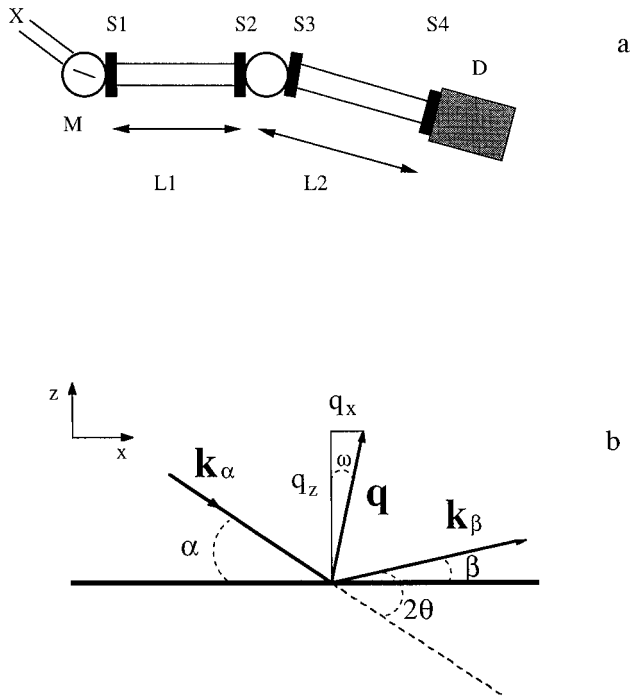

FIG. 3. (a) The experimental setup with x-ray source (X), bent graphite monochromator (M), 4 pairs of slits ($S1$,$S2$,$S3$,$S4$) and a NaI scintillation detector (D); (b) The scattering geometry; the reciprocal space wave vector transfer is defined as $\mathbf{q}=\mathbf{k}_\beta-\mathbf{k}_\alpha$.

rated by $L1=450$ mm. This leads to $\Delta\alpha=0.044°$ full width at half maximum (FWHM), which was confirmed by a detector scan of the main beam with very narrow detector slits. $S3=0.7$ mm serve to reduce background scattering. The in-plane detector acceptance $\Delta\beta=0.048$ FWHM is determined by slits $S4=0.35$ mm in front of the scintillation detector at a distance detector-sample $L2=410$ mm. A detector scan of the main beam resulted in 0.062° FWHM and could be fit to a Gaussian.

All slits were wide open vertically, while $S2$ was set at 3 mm. The beam size on the sample was approximately 0.1×3 mm^2 ($H\times V$). In the scattering configuration described we obtained an incident beam intensity of 8×10^7 counts/s. The background scattering at intermediate angles was near dark-count levels of 0.1 count/s as a result of the absence of a substrate as well as the use of an evacuated sample oven. This allowed a dynamic range of nearly nine orders of magnitude in the measured intensity, enabling to probe small in-plane length scales.

During the experiments we have taken three types of scans: specular reflectivity scans, in which α and β are varied together while keeping them equal, radial diffuse scans where α and β are varied while the sample is offset from the specular condition by a constant angle $\omega=(\beta-\alpha)/2$, and transverse diffuse (rocking) scans in which ω is varied but the total scattering angle $\alpha+\beta$ is kept fixed. In reciprocal space specular scans probe the scattered intensity along q_z with $q_x=0$, in radial diffuse scans both q_z and q_x are varied, and for small angles transverse diffuse scans probe essentially along q_x at fixed q_z.

C. Resolution

The in-plane divergences $\Delta\alpha$ and $\Delta\beta$ can be approximated by Gaussians, leading to a resolution area in the scattering plane determined by $k\Delta\alpha$ and $k\Delta\beta$. From now on, $\Delta\alpha$ and $\Delta\beta$ will be expressed as Gaussian half widths, a factor $2\sqrt{2\ln 2}$ smaller than the corresponding FWHM in Sec. III B. The wave vector transfer can be written as $\mathbf{q}=\mathbf{k}_\beta-\mathbf{k}_\alpha$, with

$$q_z=k(\sin\beta+\sin\alpha), \tag{20}$$

$$q_x=k(\cos\alpha-\cos\beta). \tag{21}$$

Differentiating with respect to α and β, while neglecting the wavelength dispersion, leads to

$$\delta q_z=k(\cos\beta\,\delta\beta+\cos\alpha\,\delta\alpha), \tag{22}$$

$$\delta q_x=k(\sin\beta\,\delta\beta-\sin\alpha\,\delta\alpha). \tag{23}$$

With the assumption that $\delta\alpha$ and $\delta\beta$ are randomly distributed, the resolution widths in q_x and q_z are given by

$$\Delta q_z=k[\cos^2\beta(\Delta\beta)^2+\cos^2\alpha(\Delta\alpha)^2]^{1/2}, \tag{24}$$

$$\Delta q_x=k[\sin^2\beta(\Delta\beta)^2+\sin^2\alpha(\Delta\alpha)^2]^{1/2}. \tag{25}$$

For this work, $\Delta\alpha\approx\Delta\beta$; such a symmetric resolution is advantageous for diffuse scattering measurements, in contrast to the case of specular reflectivity measurements for which typically $\Delta\beta\gg\Delta\alpha$ [18]. In the case of a symmetric resolution we can write for the resolution function [31]

$$R(\delta q_z,\delta q_x)=\exp[-[\delta q_z^2(\alpha^2+\beta^2)+2\,\delta q_z\delta q_x(\beta-\alpha)+2\,\delta q_x^2]/(q_z\Delta\alpha)^2]. \tag{26}$$

In general, the resolution function cannot be separated in δq_z and δq_x, which is needed for a quantitative analysis of the data. This is a result of the cross term that causes a tilt of the resolution area. This cross term disappears if we express the resolution as a function of $q_\parallel$ and $q_\perp$, where $q_\parallel$ and $q_\perp$ are the components parallel and perpendicular to $\mathbf{q}$. We get for all α and β

$$R(\delta q_\parallel,\delta q_\perp)=R(\delta q_z,\delta q_x)\big|_{\alpha=\beta}. \tag{27}$$

At small angles the Gaussian resolution half widths perpendicular and parallel to $\mathbf{q}$ are given by

$$\Delta q_\parallel=\sqrt{2}k\Delta\alpha, \tag{28}$$

$$\Delta q_\perp=(q_z/2k)\Delta q_\parallel. \tag{29}$$

Using Eqs. (28), (29) and $q_z=2k\alpha$, we can write for Eq. (26)

$$R(\delta q_\parallel,\delta q_\perp)=\exp\left(-\frac{\delta q_\parallel^2}{\Delta q_\parallel^2}\right)\exp\left(-\frac{\delta q_\perp^2}{\Delta q_\perp^2}\right), \tag{30}$$

where $\Delta q_\perp$ and $\Delta q_\parallel$ are the resolution half widths perpendicular and parallel to $\mathbf{q}$. While at small angles $q_\parallel\approx q_z\approx|\mathbf{q}|$ and $q_\perp\approx q_x$, $\Delta q_\parallel$ and $\Delta q_\perp$ differ from Δq_z and Δq_x, respectively.

For this work, $\Delta q_{\parallel}=1.9\times10^{-3}$ Å^{-1} and $\Delta q_{\perp}=2.3\times10^{-4}q_z$ Å^{-1}. Out of the scattering plane (z,x-plane) the resolution is poor due to the focusing of the monochromator and the widely set detector slits, and $\Delta q_y\simeq0.1$ Å^{-1}. Thus the intensity is effectively integrated over in this direction for the range of q_x values probed.

For proper analysis of the diffuse scattering signal, it is important that the film mosaic due to nonflatness of the holder $\Delta\omega_{\rm mos}$ is small compared to the experimental resolution, or at least that it can be considered constant over the range of the measurements. $\Delta\omega_{\rm mos}$ contributes to the resolution width in the perpendicular direction as

$$\Delta q_{\perp}^2({\rm tot})=\Delta q_{\perp}^2(\Delta\alpha,\Delta\beta)+q^2\Delta\omega_{\rm mos}^2, \tag{31}$$

while $\Delta q_{\parallel}$ remains constant. The holder flatness was determined by transverse diffuse scans at various specular positions in q_z, performed using a high resolution (Ge monochromator and analyzer) setup. It was found to be essentially constant as a function of the incident angle, and thus beam footprint. The footprint of the beam on the sample is defined by $F=b/\sin\alpha$, where b is the width of the beam at the sample position. For the largest footprint, which occurs at an incident angle $\alpha\approx0.5°$, the film mosaic is nearly Gaussian with a width $\Delta\omega_{\rm mos}=0.035°$ FWHM. The film mosaic broadens the specular peak in the transverse direction (and thus increases $\Delta q_{\perp}$) by less than 10% in the moderate resolution setup described.

D. Intensity calculation

Following Refs. [8,18], consistent with the first Born approximation but including refraction, the structure factor can be written in the form

$$S(\mathbf{q})=\left[|R_F|^2\exp(-q_z'^2\sigma_{\rm loc}^2)\int dx\ \exp(-iq_xx)G(x,q_z')\right] \tag{32}$$

with

$$G(x,q_z')=\sum_{m,n}^{N}\exp[iq_z'(m-n)d]\exp[-q_z'^2g_{mn}(x)/2]. \tag{33}$$

Here $g_{mn}(x)\equiv g(x,z_m,z_n)$, with $z_j=[j-(1/2)(N+1)]d$, is calculated using Eq. (9) and the double sum runs over all N layers. The average z component of the wave vector transfer in the film is $q_z'=(q_z^2-q_c^2)^{1/2}$, where q_c is the critical wave vector transfer for total reflection. The term $|R_F|^2$ is an exact calculation of the Fresnel reflectivity of a single layer, in which the smectic layer is approximated by the slab model of Fig. 2(b) [32]. It is smeared with a Gaussian of width $\sigma_{\rm loc}$, which approximates the local (short wavelength) contribution to the total fluctuations. The two-dimensional resolution convolution over $(\Delta q_{\parallel},\Delta q_{\perp})$ is performed as a one-dimensional convolution (denoted as $\otimes$) along $q_{\parallel}$ with half width $\Delta q_{\parallel}$, and a real space cutoff of $1/\Delta q_{\perp}$ to the structure factor integration along x, giving

$$\frac{I(\mathbf{q})}{I_0}=\left[|R_F|^2\exp(-q_z'^2\sigma_{\rm loc}^2)\,\frac{\Delta q_{\perp}}{\sqrt{2\pi}}\int_{-\infty}^{\infty}dx\times\exp(-iq_xx)\exp[-\tfrac{1}{2}x^2\Delta q_{\perp}^2]G(x,q_z')\right]\otimes\exp[-\tfrac{1}{2}q_{\parallel}^2/\Delta q_{\parallel}^2]. \tag{34}$$

The cutoff to the integral in terms of the effective coherence length allows a calculation of $g_{mn}(x)$ without use of a resolution determining cutoff as in Refs. [16,33]. Note that the cutoff to the real-space integration in Eq. (34) is only possible with a separable resolution function and leads to an expression for the intensity without an artificial separation of the specular and diffuse component. Also, note that the normalization to the integration (the term $\Delta q_{\perp}/\sqrt{2\pi}$) gives the proper $1/q_z^3$ dependence for the diffuse component.

The data were corrected for three geometrical effects that reduce the effective footprint of the beam on the sample F' and thus the scattered intensity. The first effect occurs at small incoming angles α, where the footprint F can be larger than the sample dimension along the beam. Overfilling occurred typically for $\alpha\leqslant0.2°$. In addition, when the detector angle $\beta\gg\alpha$ and α small, the sample area visible by the detector is limited by the width of $S4$, assuming a wide detector and no divergence of the beam. Finally, the films hung approximately 60 μm below the holder surface due to the thickness of the razor blades, leading to incomplete illumination of the sample due to shadowing of the holder. This occurred for incident and outgoing angles $\leqslant0.5°$. These three effects can result in $F'<F$, in which case the intensity was multiplied by the ratio F/F'.

Furthermore, intensities in transverse and radial diffuse scans were multiplied by the factor $(\sin\alpha/\sin\theta)$, to correct for the varying illuminated sample area when $\alpha\neq\beta$. Transverse diffuse scans are background subtracted. The background was calculated from scans with no film present and from data for which $\alpha\leqslant0$ or $\beta\leqslant0$. Models of the radial scans have a constant background added. All data were scaled to the main beam intensity.

E. Fitting parameters

In the fitting procedure we have three groups of significant model parameters: (N,d), (γ,K,B), and $(\sigma_{\rm loc},d_{\rm tail},\delta_{\rm tail}/\delta_{\rm core})$. All but the number of layers N are given a single value for modeling the data at all film thicknesses. The second group is related to the hydrodynamic fluctuations and the third group [see Fig. 2(b)] to the local smectic (dis) order. To appreciate the experimental results it should be realized how they depend in a qualitative way on the various parameters. The surface tension is connected with the roughness of the surfaces and thus with the overall falloff of the specular intensity along q_z, as well as with the line shape of transverse diffuse scans at small q_x. The combined effect of γ and the resolution width $\Delta q_{\perp}$ determines the ratio of specular to diffuse intensity. The bending elastic constant K is connected with the nonlinearity of the transverse line shape, when plotted on a log-log scale, at large q_x even for $B\rightarrow\infty$. Thus its effect is observable as a deviation at large q_x

from a simple power law behavior $I(q_x) \sim 1/q_x^{1-\eta}$, with $\eta = k_B T q_z^2/(4\pi\gamma)$, expected for simple liquids with surface tension [16]. For lateral length scales above R_c capillary waves dominate the fluctuations, and below this cutoff the smectic fluctuations dominate. The compression elastic constant B is determined by the value of R_c and/or the amplitude of the fluctuations. If in-plane lengths are smaller than R_c conformality is lost, which would show up in the loss of fringes in radial diffuse scans as well as in the line shapes of transverse diffuse scans across Bragg peaks compared to those at intermediate q_z positions.

The local density model used in the analysis makes no assumptions about the expected molecular density profile, but rather uses the most simple ''slab'' model [as shown in Fig. 2(b)] which can describe the layer form factor for two Bragg peaks. We assume up-down symmetry of the molecules in the smectic film and approximate a single smectic layer as consisting of regions of constant index of refraction, with a center region of a given index of refraction $n_{\rm core} = 1 - \delta_{\rm core}$ and length $d_{\rm core}$, and two identical tail regions of given index $n_{\rm tail} = 1 - \delta_{\rm tail}$ and length $d_{\rm tail}$. The layer averaged $\delta_{\rm av} = (\delta_{\rm tail} d_{\rm tail} + \delta_{\rm core} d_{\rm core})/d$ determines the critical angle, as $q_c = 2k\sqrt{2\,\delta_{\rm av}}$, and adds a scaling factor to the intensity. However shadowing effects of the film holder made it impossible to measure near q_c. The total layer spacing d is fixed by the position of the Bragg peaks, so that $d_{\rm core} = d - 2d_{\rm tail}$. Two parameters strongly influence the fitting; $\delta_{\rm tail}/\delta_{\rm core}$, which determines the strength of the Bragg peaks, and $d_{\rm tail}/d$, which affects the relative strength of the second to the first Bragg peak. These parameters show very little interdependence.

Finally, a Gaussian smearing of width $\sigma_{\rm loc}$ is included to the local layer profile. The various contributions to the fluctuations are assumed to be independent Gaussian random variables and are related by $\sigma_{\rm tot}^2 = \sigma_{\rm loc}^2 + \sigma^2$. Here $\sigma_{\rm tot}$ is the specular falloff given by $\exp(-q_z^2 \sigma_{\rm tot}^2)$ and $\sigma = \sigma(0,z)$ is determined by the hydrodynamic fluctuations as fit to the transverse diffuse scans. A Gaussian smearing with width $\sigma_{\rm loc}$ will lead to an overall falloff of the specular intensity, more strongly with increasing q_z.

IV. EXPERIMENTAL RESULTS

Figure 4 shows specular (at $q_x = 0$) and radial diffuse scans (measured along $q_x = 2.62 \times 10^{-3} q_z$ and $q_z = 1.31 \times 10^{-2} q_z$) for films of 3, 6, 20, and 34 layers. The 3 layer film only lasted long enough to complete the two radial scans shown. Note the similarity of the specular and diffuse radial scans indicating conformality between the interfaces over the in-plane length scales measured. Transverse diffuse scans were done across the first and second Bragg peaks and across two intermediate q_z positions at interference fringes. Figure 5 shows transverse diffuse scans for films of 4, 20, and 34 layers. Note the excellent agreement of the line shapes at $\pm q_x$, as a result of the symmetric resolution.

The positions of the Bragg peaks and the Kiessig fringes in the specular reflectivity curve fix d and N, respectively. We find $d = 29.40 \pm 0.04$ Å, independent of layer position and film thickness. With the obtained N and d, the transverse line shapes at fixed q_z were fit, for each film separately, varying only γ, K, and B. Best fits for all films occur for values of $\gamma = (13.0 \pm 0.5) \times 10^{-3}$ N/m, $K = (1.0 \pm 0.5) \times 10^{-11}$ N, and $B = (7.5 \pm 2.5) \times 10^{8}$ N/m^2. Fits using these values are given as the solid lines in Fig. 5. Fits to the specular scans (Fig. 4) were then performed with only the third group $(\sigma_{\rm loc}, d_{\rm tail}, \delta_{\rm tail}/\delta_{\rm core})$ as adjustable parameters, using the obtained values of γ, B, and K in Eq. (34). We find $\sigma_{\rm loc} = 2.6$ Å, $d_{\rm tail} = 0.19d$, and $\delta_{\rm tail}/\delta_{\rm core} = 1.14$. These values are essentially independent of both layer number and film thickness. Finally fits to the radial diffuse scans could be made using the above obtained set of parameters, without further adjustments.

V. DISCUSSION

Let us first discuss the results for the various parameters as obtained from the analysis. The value of 13×10^{-3} N/m obtained for the surface tension is smaller than the values reported so far, which lie in the range $(20\text{–}26) \times 10^{-3}$ N/m [34]. However, a recent direct measurement of the surface tension of FPP was done after completion of our work, giving $(12.5 \pm 0.5) \times 10^{-3}$ N/m [35]. Values in the same range were found for other fluorinated compounds. Apparently, fluorination of an alkyl chain of liquid crystals leads to a considerable reduction of the surface energy [36]. The value obtained for K is quite normal compared to other systems [1]. On the other hand, the value of B is about two orders of magnitude larger than values reported for other smectic-A systems [37]. However, most of these published data were taken close to a second order smectic-A to nematic phase transition, where $B \to 0$. This could easily explain an order of magnitude difference with our situation. Another order of magnitude might be a result of the fluorinated chain, which is bulkier and stiffer than a hydrogenated chain. In fact, the average cross section of a fluorinated tail is approximately 30% larger than that of a hydrocarbon chain [38]. In addition, *gauche* conformers can practically be excluded, leading to rigid rodlike fluorinated chains [39]. The resulting structural molecular model consists of a rigid aromatic core with a flexible hydrocarbon tail on one side and a rigid fluorinated tail on the other side.

Clearly our FPP system is nearly incompressible, with layers fluctuating in unison down to the shortest in-plane wavelengths measured. This leads to $R_c \approx 20$ Å for a 34 layer film, which is of the order of molecular dimensions. Thus loss of conformality of the fluctuations can only be expected for unrealistically large q values or much thicker films. The transverse diffuse intensity for the 4 layer film has a logarithmic dependence at all q_x values measured, in agreement with $\log_{10}(1/R_l) \approx -1.3$ Å^{-1} as calculated using Eq. (16). For the 20 and 34 layer film $\log_{10}(1/R_l)$ is equal to -1.7 and -1.8, respectively, just within the accessible q range. Indeed, deviations from the logarithmic dependence can be seen in the bottom curves of Fig. 5(b) and 5(c) (at the second Bragg peak). Films of different thicknesses have a different sensitivity to the various parameters. The larger logarithmic range of the transverse data for thin films results in a very accurate determination of γ. However the data for the 4 and 6 layer film gives only a lower limit of $B = (7.5 \pm 2.5) \times 10^{8}$ N/m^2 and could equally well be fit using Eq. (19) derived for $B \to \infty$. Thicker films are necessary to determine the actual

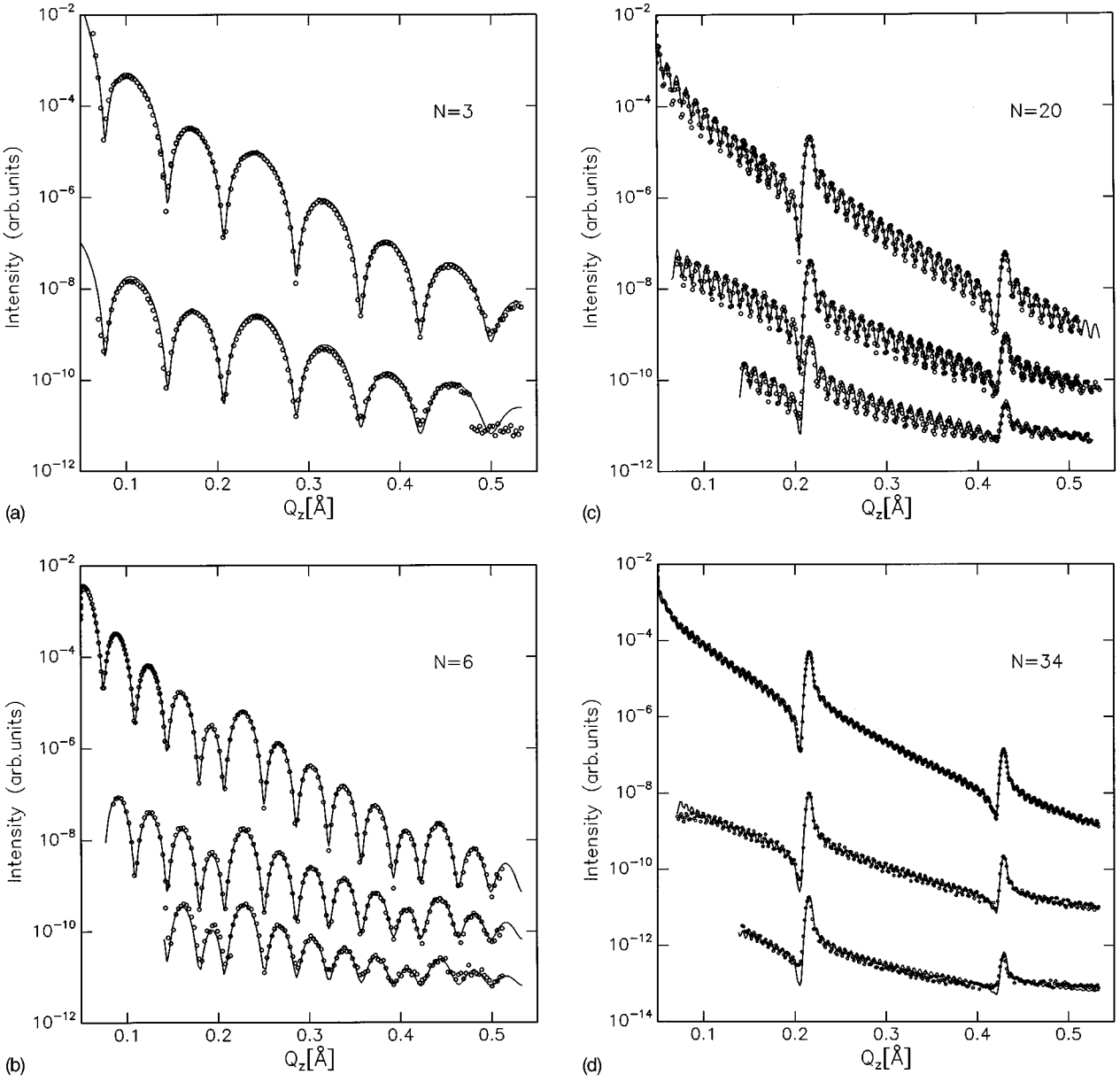

FIG. 4. Specular (ω=0, upper curves) and diffuse (ω=0.15°, middle curves and ω=0.75°, lower curves) radial scans, with solid line fits as described in the text. Curves have been shifted for clarity; (a) 3 layer film; (b) 6 layer film; (c) 20 layer film; (d) 34 layer film.

value of B. The effect of a variation of B is illustrated in Fig. 6 for the 34 layer film. It is apparent that changing B by an order of magnitude can only lead to worse fits.

Finally we come to the third group of parameters containing all the local information. The value of σ_{loc}=2.6 Å for the local fluctuations, which is independent of the film thickness, can be compared with σ_{tot} as obtained from a standard slab model fit to the specular reflectivity [40]. This total fluctuation amplitude has a contribution of both the thermal fluctuations and the local molecular disorder. We find that σ_{tot} is almost independent of the film thickness, being 4.8 Å for the 4 layer film and 4.5 Å for the 34 layer film. Using $\sigma_{tot}^2=\sigma^2+\sigma_{loc}^2$ gives values of σ=4.1 Å and σ=3.7 Å, respectively, for the hydrodynamic part of the fluctuations. Evidently the local fluctuations add a non-negligible contribution to the total fluctuation profile for FPP and the common belief that these can be neglected [7,8,14] is not generally valid. Recent measurements on a nonfluorinated liquid crystal with a similar analysis resulted in σ_{loc}=1.1 Å, indicating that the large value of σ_{loc} for FPP is not an artifact of the simple slab model used to describe the molecule.

The agreement between the model and the data for the fluorinated liquid crystal investigated is remarkable, using the same parameters for every thickness film. It should be noted that the value of the layer spacing d=29.4 Å was independent of the film thickness as well as the position of the layer in the film. Allowing smaller d spacings for the surface layers assuming tilted top layers, because of the presence of a smectic-C phase for FPP at lower temperatures, made the quality of the fits worse. This even applies to the thinnest films. As opposed to Ref. [36] the data could not be modeled assuming polar ordering at the surface.

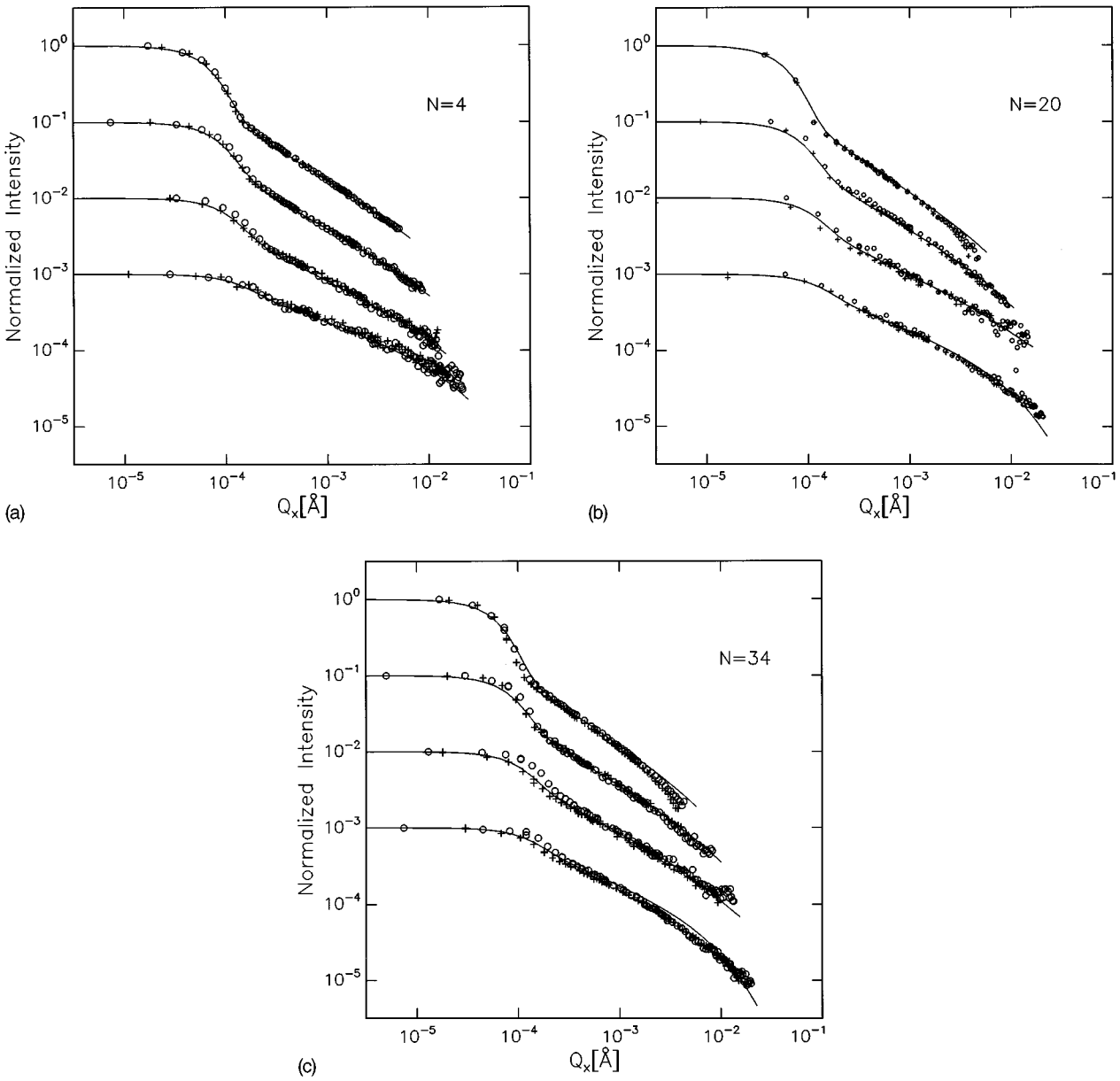

FIG. 5. Transverse diffuse scans at fixed q_z, with solid line fits as discussed in the text; circles and crosses indicate positive and negative q_x, respectively; (a) 4 layer film with from top to bottom q_z-values of 0.235, 0.292, 0.348, and 0.448 Å^{-1}; (b) 20 layer film with q_z values of 0.216, 0.287, 0.355, and 0.429 Å^{-1}; (c) 34 layer film with q_z values of 0.216, 0.292, 0.363, 0.427 Å^{-1}. Curves have been shifted for clarity.

The best fits were obtained for the thinnest films where the continuum model is assumed to be less valid. However, the data exhibits deviations from the model for thicker films at higher q values. This is most evident in the transverse line shapes at the Bragg positions [Fig. 5(c) top and bottom curves], where varying B and K did not improve the fits. Off-Bragg peak transverse diffuse scans of the same film [Fig. 5(c) middle curves] agree better with the model. The Bragg positions are characterized by constructive interference of all the layers. Thus the deviations could indicate that the mechanism of coupled fluctuations across smectic layers is more complicated than that incorporated in the model.

The values obtained for γ, B, K result in $\lambda=\sqrt{K/B}=1.2$ Å, an order of magnitude smaller than the layer spacing [8]. Furthermore $\nu=0.15$, and the profile of the hydrodynamic (collective) fluctuations along z is quite flat and nearly independent of N, as can be expected for a system with a high B and low γ [8]. However, as $\nu<1$ an enhancement of the surface fluctuations as compared to the interior of the film should be anticipated. Figure 7 shows the fluctuation amplitude as a function of z, at large R where the correlation term is negligible, calculated using Eq. (A10). Indeed, a slight enhancement of the surface fluctuations is observed.

Figure 8 shows the molecular form factor calculated using the slab model of Fig. 2(b) with the fit parameters for a 34 layer film. In addition, the form factor calculated by Fourier transforming the electron density profile of an up-down symmetric molecule projected onto the z axis [41] is shown as

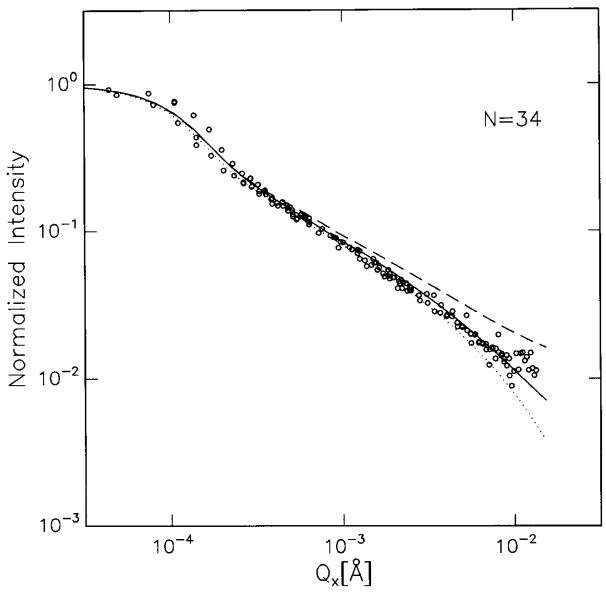

FIG. 6. Calculation of the scattered intensity in a transverse diffuse scan for a 34 layer FPP film at $q_z = 0.355$ Å^{-1}, with $B = 10^8$ N/m^2 (dashed line), 7.5×10^8 N/m^2 (solid line) and 5×10^9 N/m^2 (dotted line).

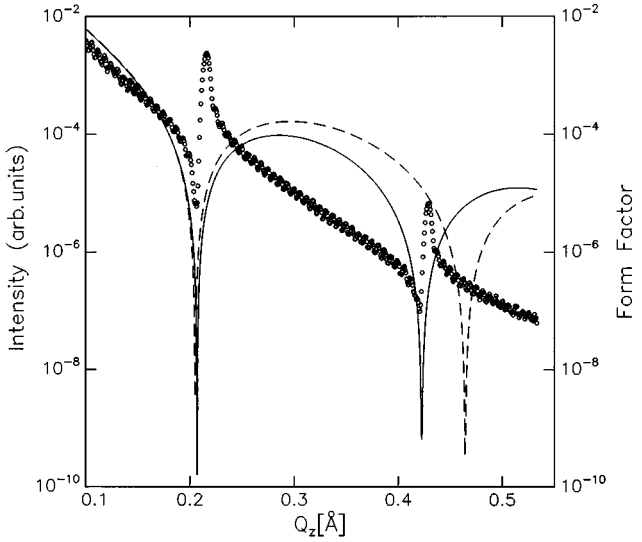

FIG. 8. Specular reflectivity curve of a 34 layer FPP film and the molecular form factor as obtained from the fit (solid line) and as calculated for an up-down symmetric molecule (dotted line). Curves have been shifted.

the dashed line. The molecular form factor as obtained from the fit differs considerably from the calculation with respect to the following points. First, the layer spacing $d = 29.4$ Å is larger than the length of the molecule $l = 27.7$ Å. This is in agreement with previous measurements on other fluorinated liquid crystals [39]. Second, the fitted value of d_{tail} is $0.19d$ ($d_{\text{core}} = 0.62d$), while from the calculation $d_{\text{tail}} \approx 0.30d$ ($d_{\text{core}} = 0.40d$) would be expected. Finally, $\delta_{\text{tail}}/\delta_{\text{core}}$ is 1.14, where a difference between δ_{tail} and δ_{core} of the order of 50% would be expected from the simple model. We emphasize that the fit parameters are hardly coupled (see Sec. III E). For example, when $d_{\text{core}} = 0.5d$, the form factor has a minimum at the position of the second Bragg peak, which then will be absent. In the case of FPP the minimum is positioned at the low q side relative to the second Bragg peak indicating that $d_{\text{core}} > 0.5d$. The observed minimum relative to the position of the *first* Bragg peak is a result of the presence of a high electron density region $\delta_{\text{tail}} > \delta_{\text{core}}$ for FPP at the air-film interface. The experimental findings for the molecular form factor can be explained with a model of antiparallel overlapping FPP molecules, a smectic-A_d phase, where the bulky fluorinated tails do not overlap with the hydrogenated chains. As a result $\delta_{\text{tail}}/\delta_{\text{core}}$ decreases and d_{core} is longer. This will be the subject of a future paper.

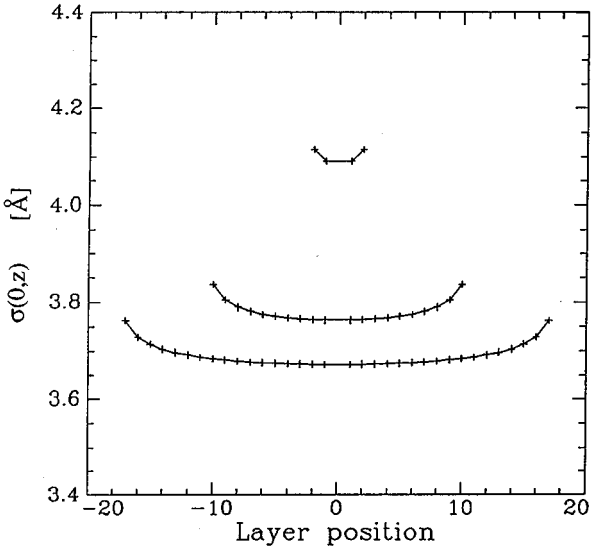

FIG. 7. The thermal fluctuation profile for a 4, 20, and 34 layer FPP film, respectively.

The measurements of the displacement-displacement correlations presented here, shed new light on earlier results for freely suspended smectic films. Previous measurements [14] of the fluctuation profile using specular reflectivity could only test certain aspects of the Holyst theory, because the specular reflectivity is only sensitive to the laterally averaged electron density profile, and cannot distinguish between long-wavelength fluctuations and the local disorder. Also, the specular scattering is essentially unaffected by the correlations $\langle u(r)u(0)\rangle$, which in fact for the previous work were assumed to be zero. We stress that it is essential to use a combination of diffuse and specular scattering in order to determine the total fluctuation profile.

VI. CONCLUSION

We have quantitatively determined the correlations of the thermal fluctuations in thin freely suspended smectic-*A* films. This is accomplished by measuring, via the diffuse x-ray scattering, the in-plane wave vector dependence of the hydrodynamic (collective) fluctuations which are governed by the elastic parameters of the liquid crystal. This is to be

contrasted with results reported so far restricted to the specular scattering, which depends only weakly on the correlations of the fluctuations. The combination of diffuse and specular scattering measurements also enables separation of the contribution of the collective thermal fluctuations and the local smectic disorder. In contrast to the usual assumptions we found the latter to be non-negligible.

The data were interpreted using a continuous model for the calculation of the displacement-displacement correlation function. With a proper cutoff it is equivalent to the previous models of Holyst [7–9]. We show that there are two characteristic in-plane lengths; if $R>R_l$ the correlation function depends logarithmically on R with a prefactor that only depends on the surface tension, while for $R>R_c$ all the layers fluctuate in unison.

All data (specular, radial diffuse and transverse diffuse scans) could be modeled using a single set of parameters. All films we measured of the fluorinated compound, with thicknesses varying from 4 to 34 layers, were conformal down to the smallest in-plane length scales probed. We show that in order to analyze the data quantitatively, it is essential to use a symmetric, separable resolution function, so that separation of the specular and diffuse contribution to the scattered intensity can be avoided. The separability of the resolution function also allows a calculation of the correlation function without a resolution determining cutoff as well as a simple normalization of the intensity.

ACKNOWLEDGMENT

We acknowledge C. C. Huang for providing the results of the direct surface tension measurements of FPP. This work is part of the research program of the Stichting voor Fundamenteel Onderzoek der Materie [Foundation for Fundamental research on Matter (FOM)] and was made possible by financial support from the Nederlandse Organisatie voor Wetenschappelijk Onderzoek [Netherlands Organisation for the Advancement of Research (NWO)]. A. N. S. acknowledges partial financial support from INTAS under Grant No. 94-4078.

APPENDIX: THE DISPLACEMENT-DISPLACEMENT CORRELATION FUNCTION

The purpose of this section is to compare the three existing methods of calculating the displacement-displacement correlation function $C(R,z,z')=\langle u(\mathbf{R},z)u(0,z')\rangle$ for freestanding smectic films. As mentioned in Sec. II the original formulation by Holyst [8] is a discrete version of the theory. Subsequently two different continuous version were published [9,10]. In this paper we have elaborated on the formulation of Ref. [10]. The starting point of all considerations is the free energy in the Gaussian approximation as given by Eqs. (1) and (2). The most convenient approach is to calculate $C(R,z,z')$ in the $(\mathbf{Q},z,z')$ representation and subsequently take the inverse Fourier transform with respect to $\mathbf{Q}$. Substituting

$$u(\mathbf{Q},z)=\int d\mathbf{R}\ \exp[-\imath\mathbf{Q}\cdot\mathbf{R}]u(\mathbf{R},z) \tag{A1}$$

in Eqs. (1) and (2) yields

$$F=\frac{1}{(2\pi)^2}\int d\mathbf{Q}\ F_{\mathbf{Q}}, \tag{A2}$$

with

$$F_{\mathbf{Q}}=\frac{1}{2}\int_{-L/2}^{L/2}dz[B|\partial_z u(\mathbf{Q},z)|^2+KQ^4|u(\mathbf{Q},z)|^2]$$

$$+\frac{1}{2}Q^2\gamma[|u(\mathbf{Q},z=L/2)|^2+|u(\mathbf{Q},z=-L/2)|^2]. \tag{A3}$$

The approach of Ref. [8] deals with a finite set of discrete values $u_j(\mathbf{Q})$, corresponding to the displacements of the layers. The second one [9] is based on a continuous representation of $u(\mathbf{Q},z)$ in the form

$$u(\mathbf{Q},z)=u_0(\mathbf{Q},z)+\delta u(\mathbf{Q},z), \tag{A4}$$

where u_0 satisfies an Euler-Lagrange equation for the bulk and δu vanishes at the surfaces. The function u_0 is fixed by two parameters, $u(\mathbf{Q},z=\pm L/2)$, while δu can be expanded in a series of orthogonal functions. Such a representation allows one to use the equipartition theorem and finally, after taking the inverse Fourier transform, yields

$$\langle u(\mathbf{R},z)u(0,z')\rangle=\frac{k_BT}{4\pi\sqrt{KB}}\int_{\xi_1}^{\xi_0}d\xi J_0(\sqrt{\xi}\varrho)\left\{\frac{e^{-\xi}}{\xi}\left[\frac{\cosh(z_+/L)+\cosh(z_-/L)}{\nu(1+e^{-\xi})^2+1-e^{-2\xi}}+\frac{\cosh(z_+/L)-\cosh(z_-/L)}{\nu(1-e^{-\xi})^2+1-e^{-2\xi}}\right]\right.$$

$$\left.+\sum_{n=1}^{N-1}\frac{\cos[\pi n(z_-/L)]+(-1)^{n-1}\cos[\pi n(z_+/L)]}{\xi^2+(\pi n)^2}\right\}. \tag{A5}$$

Here $\xi = LQ^2\lambda$, $\xi_0 = L\lambda(2\pi/a_0)^2$, $\xi_1 = L\lambda(2\pi/W)^2$, where a_0 is the molecular diameter and W the in-plane size of the system. Apart from some rewriting and differences in notation, this expression results directly from Ref. [9]. It leads to a correlation function which coincides with that of Ref. [8] within 5%.

The third approach developed in Ref. [10] is based on the expression

$$\langle u(\mathbf{Q},z)u^*(\mathbf{Q},z')\rangle = \frac{\int u(\mathbf{Q},z)u^*(\mathbf{Q},z')\exp(-F_Q/k_BT)Du}{\int \exp(-F_Q/k_BT)Du}. \tag{A6}$$

All the integrals involved are well defined if F_Q is of the form $1/2(u,\hat{A}u)$, $\hat{A}$ being a self-adjoint positive operator. In this case the correlation function can be written as

$$\langle u(\mathbf{Q},z)u^*(\mathbf{Q},z')\rangle = k_BT\hat{A}^{-1}(z,z'). \tag{A7}$$

The operator $\hat{A}$ and its domain must satisfy the following conditions. First, $1/2(u,\hat{A}u)$ must coincide with F_Q for any arbitrary u from the domain. Second, $\hat{A}$ must be self-adjoint so that an arbitrary function can be expanded into its complete set of eigenfunctions. Third, all the eigenvalues must be positive, in order that the integrals in Eq. (A6) converge. One can prove that the operator

$$\hat{A} = -B\partial_z^2 + KQ^4 \tag{A8}$$

acting on functions $u(\mathbf{Q},z)$ defined by the boundary conditions

$$\gamma Q^2 u(\mathbf{Q},\pm L/2) \pm B\partial_z u(\mathbf{Q},\pm L/2) = 0 \tag{A9}$$

fulfills all the requirements. Using a compact expression for the inverse operator [10], we obtain

$$\langle u(\mathbf{R},z)u(0,z')\rangle = \frac{k_BT}{8\pi\sqrt{KB}}\int_{\xi_1}^{\xi_0} d\xi \times \frac{J_0(\sqrt{\xi}\varrho)}{\xi[(1+\nu)^2-(1-\nu)^2e^{-2\xi}]} \times f(\xi,z_+,z_-), \tag{A10}$$

where the function f is given by Eq. (7). A simple analysis based on the identity

$$\sum_{n=1}^{\infty} \frac{\cos(\pi n z_-/L)+(-1)^{n-1}\cos(\pi n z_+/L)}{\xi^2+(\pi n)^2} = \frac{1}{2\xi[1-e^{-2\xi}]}\times\{\exp(-\xi z_-/L)+\exp(-\xi(2-z_-/L)) - 2e^{-\xi}\cosh(z_+/L)\} \tag{A11}$$

shows that Eq. (A5) and Eq. (A10) differ by an additional cutoff in the z direction introduced into Eq. (A5) by cutting the summation. As a result, Eq. (A5) gives a slightly smaller magnitude of the mean-square fluctuations than our treatment. As the layers have a finite thickness and, furthermore, there is a smearing of the layers because of the thermal motion of the molecules, the z coordinate of a single layer is not defined precisely. Thus it seems necessary to incorporate a cutoff in the z direction into our formulation as well. It turns out that a minimal magnitude $z_0 = d/4$ for z_- (instead of zero) in Eq. (A10) gives results identical to Eq. (A5). All calculations presented have been done with this choice of z_0.

[1] See, for example, G. Vertogen and W. H. de Jeu, *Thermotropic Liquid Crystals, Fundamentals* (Springer, Berlin, 1988).
[2] J. Als-Nielsen, J. D. Litster, R. J. Birgeneau, M. Kaplan, C. R. Safinya, A. Lindegaard-Andersen, and S. Mathiesen, Phys. Rev. B **22**, 312 (1980).
[3] G. Friedel, Ann. Phys. (N.Y.) **18**, 273 (1922).
[4] C. Y. Young, R. Pindak, N. A. Clark, and R. B. Meyer, Phys. Rev. Lett. **40**, 773 (1978).
[5] C. Rosenblatt, R. Pindak, N. A. Clark, and R. B. Meyer, Phys. Rev. Lett. **42**, 1220 (1979).
[6] P. S. Pershan, *Structure of Liquid Crystal Phases* (World Scientific, Singapore, 1988).
[7] R. Holyst, D. J. Tweet, and L. B. Sorensen, Phys. Rev. Lett. **65**, 2153 (1990).
[8] R. Holyst, Phys. Rev. A **44**, 3692 (1991).
[9] A. Poniewierski and R. Holyst, Phys. Rev. B **47**, 9840 (1993).
[10] A. N. Shalaginov and V. P. Romanov, Phys. Rev. E **48**, 1073 (1993).
[11] V. P. Romanov and A. N. Shalaginov, Zh. Eksp. Teor. Fiz. **102**, 884 (1992) [Sov. Phys. JETP **75**, 483 (1992)].
[12] G. S. Smith, C. R. Safinya, D. Roux, and N. A. Clark, Mol. Cryst. Liq. Cryst. **144**, 235 (1987).
[13] S. Gierlotka, P. Lambooy, and W. H. de Jeu, Europhys. Lett. **12**, 341 (1990).
[14] D. J. Tweet, R. Holyst, B. D. Swanson, H. Stragier, and L. B. Sorensen, Phys. Rev. Lett. **65**, 2157 (1990).
[15] J. D. Shindler, E. A. L. Mol, A. N. Shalaginov, and W. H. de Jeu, Phys. Rev. Lett. **74**, 722 (1995).
[16] M. K. Sanyal, S. K. Sinha, K. G. Huang, and B. M. Ocko, Phys. Rev. Lett. **66**, 628 (1991).
[17] I. M. Tidswell, T. A. Rabedeau, P. S. Pershan, and S. D. Kosowsky, Phys. Rev. Lett. **66**, 2108 (1991).
[18] S. K. Sinha, E. B. Sirota, S. Garoff, and H. B. Stanley, Phys. Rev. B **38**, 2297 (1988).
[19] For an overview, see *Surface x-ray and Neutron Scattering*, Springer Proceedings in Physics, Vol. 61, edited by H. Zabel and I. K. Robinson (Springer-Verlag, Berlin, 1992).
[20] V. Holy and T. Baumbach, Phys. Rev. B **49**, 10668 (1994).
[21] R. Schlatmann, J. D. Shindler, and J. Verhoeven, Phys. Rev. B **51**, 5345 (1995).

[22] D. E. Savage, J. Kleiner, N. Schimke, Y. H. Phang, T. Janowski, J. Jacobs, R. Kariotis, and M. G. Lagally, J. Appl. Phys. **69**, 1 (1991).
[23] J. Daillant and O. Bélorgey, J. Chem. Phys. **97**, 5824 (1992); **97**, 5837 (1992).
[24] R. E. Geer, R. Shashidhar, A. F. Thibodeaux, and R. S. Duran, Phys. Rev. Lett. **71**, 1391 (1993).
[25] R. E. Geer and R. Shashidar, Phys. Rev. E **51**, R8 (1995).
[26] P. G. de Gennes and J. Prost, *Physics of Liquid Crystals* (Clarendon, Oxford, 1993).
[27] A. Caillé, C. R. Acad. Sci. Ser. B **247**, 891 (1972).
[28] L. Gunther, Y. Imry, and J. Lajzerowich, Phys. Rev. A **22**, 1733 (1980).
[29] I. S. Gradshteyn and I. M. Ryzhik, *Table of Integrals, Series and Products* (Academic, New York, 1980).
[30] J. D. Shindler and R. M. Suter, Rev. Sci. Instrum. **63**, 5343 (1992).
[31] W. H. de Jeu, J. D. Shindler, and E. A. L. Mol, J. Appl. Cryst. (to be published).
[32] L. G. Parrat, Phys. Rev. **95**, 359 (1954).
[33] P. Dutta and S. K. Sinha, Phys. Rev. Lett. **47**, 50 (1981).
[34] T. Stoebe, P. Mach, and C. C. Huang, Phys. Rev. E **49**, R3587, (1994).
[35] C. C. Huang (private communication).
[36] J. Pang and N. A. Clark, Phys. Rev. Lett. **73**, 2332 (1994).
[37] M. Benzekri, J. P. Marcerou, H. T. Nguyen, and J. C. Rouillon, Phys. Rev. B **41**, 9032 (1990).
[38] T. P. Rieker and E. J. Janulis, Liq. Cryst. **17**, 681 (1994).
[39] T. A. Lobko, B. I. Ostrovski, A. I. Pavluchenko, and S. N. Sulianov, Liq. Cryst. **15**, 361 (1993).
[40] M. Knewtson, R. M. Suter, and J. Shindler, Reflectivity analysis program SPEEDO.
[41] E. F. Gramsbergen, W. H. de Jeu, and J. Als-Nielsen, J. Phys. **47**, 711 (1986).